Thermal evolution of the oceanic lithosphere: an alternative view

M.P. Doin [*], L. Fleitout

URA CNRS 1316, Laboratoire de Geologie, E.N.S. 24 rue Lhomond, 75005 Paris, France

Abstract

The most common model used for representing the evolution with age of the oceanic lithosphere is the 'plate model' where the temperature is set at a fixed depth, called the base of the plate. This 'base of the plate' has no physical meaning but this model provides a mathematical substitute for a system where small-scale convection occurs through instabilities growing at the base of the cooling lithosphere and becomes effective only below old ocean. Another possible view is that convection provides heat at the base of the lithosphere whatever the age of the overlying plate. This last process can be modeled by a Constant Heat flow Applied on the Bottom Lithospheric ISotherm (CHABLIS model). A good fit to the observables (bathymetry and geoid as function of age, and old age heat-flow) can be obtained both for plate and CHABLIS models in spite of an experimentally determined thermal expansion coefficient much larger than assumed in previous plate models. These models have important consequences for several geodynamic processes. The plate, at an age of 100 Ma is only 80 km thick for both models: melting above a hot-spot can then occur in the garnet–spinel transition field without much plate thinning. In the plate model the subsidence is stopped at an age of about 80 Ma while, according to the CHABLIS model, several hundred meters of subsidence are expected after 100 Ma. Thus the two models predict quite a different long-term pattern of subsidence in the sedimentary basins. Finally, in the CHABLIS model, the global cooling of the mantle coming from cold material eroded by secondary convection at the base of the plates is considerably larger than in plate models: it amounts to 40%, the remaining 60% being due to the subduction process.

Keywords: lithosphere; oceanic crust; cooling; heat flow; thermal history

1. Introduction

The thermal evolution of the oceanic lithosphere is one of the most classical problems in Geodynamics [1–8]: If no heat is brought by convection to the base of the lithosphere, the solution corresponds to the 'half-space' cooling model. The bathymetry is predicted to be proportional to the square root of age while the geoid anomaly decreases proportionally to the age of the lithosphere. In fact, both topography [4] and geoid [9–12] are observed to flatten at old ages and the flattening of the geoid is observed at short wavelengths. The flattening of the topography occurs on very slow plates, such as the African plate. This means that these flattenings cannot be due to a dynamic effect but, rather, to heat brought to the base of the lithosphere.

Most of previous models assume that heat is brought to the base of the lithosphere and that topography departs from the square root of age law only at old ages. However, this has not been well assessed.

* Corresponding author. Tel: +33 1 44 32 22 01 Fax: +33 1 44 32 22 00. E-mail: fleitout@geophy.ens.fr

In their study of topography versus age, Colin and Fleitout [13] used two types of law: one with a shape $a + b\sqrt{age} - c \cdot age^2$, mimicking a heat transfer mainly at old ages and another one with shape $a + b\sqrt{age} - c \cdot age$, thought to mimic heat transfer independent of the age of the plate. The subsidence laws obtained (respectively $2691 + 328\sqrt{age} - 0.046 \cdot age^2$ and $2452 + 452\sqrt{age} - 15 \cdot age$) provide an equally good fit to the topography data. The coefficient b is, however, much larger with the second law, implying a thermal expansivity or conductivity very different from those currently used. The data on the geoid slope versus age [9,10] are noisy but seem to indicate an early departure from the half-space model.

In this paper, we reassess the origin and implications of the commonly used 'plate model' and propose to test a model where a heat-flow independent of age is brought to the base of the lithosphere (Section 2. In Section 3, the experimental constraints on the thermal parameters are taken into account and the observed topography, geoid and heat-flow are compared with those predicted by the two types of models. In Section 4, we discuss the implications of these models for the global cooling of the mantle, the long term subsidence of basins and the interaction of hot-spots with the lithosphere.

2. Two classes of thermal models

2.1. The plate model and other models with heat transfer at old ages

The model most commonly used to describe the thermal evolution of the lithosphere with age is the plate model: a temperature is imposed at a fixed depth, called the base of the plate. In the early stages, the thermal evolution of the lithosphere is similar to the cooling of a half-space. However, when the thermal perturbation reaches the base of the plate, heat transfer between the mantle and the plate limits the lithospheric growth. The 'base of the plate' has sometimes been considered as a real physical barrier, the matter above the depth characteristic of the base of the plate being very viscous, even when hot, and the matter below being soft, even

when cold [14]. No explanation has been given up to now as to what could be the physical mechanism for such a rheological barrier. However, it will be argued in the discussion that the buoyancy and high viscosity expected for the depleted material may provide such a barrier to convection at a depth of the order of 80 km. In models where realistic temperature-dependent viscosity is used [15,16], instabilities growing at the base of the lithosphere lead to mature convection at a critical age, which depends upon the viscosity below the plate, but which may be of the order of 70 Ma for appropriately chosen mechanical properties, leading to a lithospheric evolution similar to that predicted by the plate model. The plate model may then simply be considered as a simple mathematical parameterization for a system where heat would only be brought at the base of the plate at old ages and where the thermal boundary layer could not exceed a maximum thickness.

2.2. Models with a constant heat transfer at the base of the lithosphere

In systems where the viscosity depends both on pressure and temperature, however, the notion of critical age becomes fuzzy [15,17]. The lithosphere can destabilize early and continue to grow considerably after the onset of convection [17,18]. Moreover, secondary convection caused only by cold, sinking blobs is not necessarily realistic. If no heat is transferred from a lower boundary layer or by radioactive heating, the mantle cools at an unrealistically high rate. Reheating of the mantle material must compensate for this cooling. It is very likely in the case of one-layer mantle convection, and necessary in the case of two-layer convection, that this reheating occurs through hot rising currents, which at least partly reach the upper boundary layer. As pointed out by Fleitout and Yuen [18], convection fed from a lower boundary layer has no reason to be quenched when situated below a young plate. Indeed, lineations in the geoid visible at young ages have been interpreted as potential traces of small-scale convection [19–21].

In summary, convective heat transfer at the base of the lithosphere beginning at young ages is possible and therefore worth testing. Full convection models involving such a heat transfer have been per-

formed [18]. However, the exact geometry of the secondary convection is still speculative. In order to achieve simple models which do not involve the geometry of the convection below directly, we parameterize the heat transfer between the lithosphere and the underlying mantle using a Constant Heat-flow Assigned on the Bottom Lithospheric ISotherm. This model will be here after referred to as the 'CHABLIS model'.

Such models have already been proposed using either analytical approximations or numerical solutions [22–24]. Here, because temperature- and pressure-dependent thermal parameters are considered, this Stephan problem is solved numerically using a finite difference method. For reasons discussed in Appendix A, we neglect possible topographic perturbations due to temperature variations deeper than the base of the lithosphere and compute topography anomalies from local isostasy. Through a careful examination of both observational data (topography, heat-flow and geoid) and experimentally determined thermal parameters, we want to examine the geophysical consequences of both models.

2.3. Some characteristics of the CHABLIS model

For parameters independent of temperature and pressure, the non-dimensional topography and heat-flow as function of age computed for the CHABLIS model take a unique shape (see Appendix B). Fig. 1 shows that at young ages the topography fits quite accurately a function:

$$\text{Topo} = -a\sqrt{\text{age}} + b \cdot \text{age} \tag{1}$$

while the surface heat-flow is:

$$q_s = c/\sqrt{\text{age}} + (1 - b) \tag{2}$$

where a and c are the same as for the cooling of an infinite half-space (i.e., $a = 2/\sqrt{\pi}$ and $c = 1/\sqrt{\pi}$) and where $b = 0.724$. Eq. (1) and Eq. (2) correspond to the analytical solutions which would be obtained for a heat-flow imposed at the base of a plate, which would deepen proportionally to the square root of age (Appendix B. Eq. (1) is a simple consequence of Eq. (2).

As a consequence of Eq. (1), for a given set of thermal parameters (α, k, C_p) the topography at young ages varies less quickly for the CHABLIS model
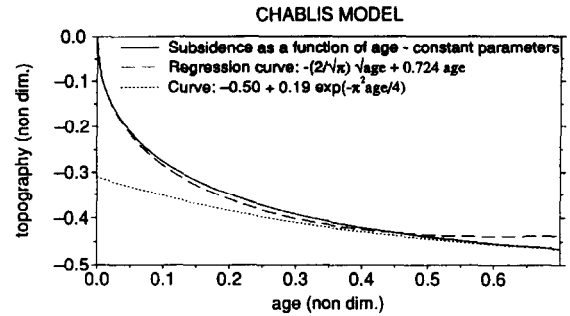

Fig. 1. Topography predicted for the CHABLIS model versus age (non-dimensional units — see Appendix B) compared with the curve $-(2/\sqrt{\pi})\sqrt{\text{age}} + 0.724 \cdot \text{age}$. The long term subsidence predicted by the CHABLIS model is fitted with an exponential law: topo $= a \exp(-\pi^2 \text{age}/4)$.

than for the plate model. (α,k, and C_p are the thermal expansion coefficient, the conductivity, and the heat capacity, respectively). The topography slope is proportional to $\alpha T\sqrt{\kappa}$. Therefore, when one tries to fit the observed topography slope at young ages, the product $\alpha T\sqrt{\kappa}$ providing a good fit for the CHABLIS model is larger than that appropriate for the plate model, as already noted in previous studies [17,22].

As shown on Fig. 1 and discussed in Appendix B, the long term subsidence for the CHABLIS model (non-dimensional topography proportional to $\exp(-\pi^2 \text{age}/4)$ is four times slower than for the plate model (non-dimensional topography proportional to $\exp(-\pi^2 \text{age})$ [23,24].

3. Fit to the observables

3.1. Fit to topography and heat-flow in the parameter space

In this section, the range of asymptotic plate thickness, mantle temperature and thermal parameters providing the best fit to the observed topography and heat-flow are inverted. The two best constraints on the evolution of the thermal lithosphere are the bathymetry as a function of age and the heat-flow at old ages. The bathymetric data set ETOPO5, sampled at 1° intervals, is corrected for the sediment load using the same file as in Colin and Fleitout [13]. The shallowest points (those which are shallower than

Table 1
Values of the thermal parameters characteristic of the Parsons and Sclater model [4] and of the GDH1 model [5]

Parameter	Parsons and Sclater model	GDH-1 model
α (K^{-1})	$3.2 \cdot 10^{-5}$	$3.1 \cdot 10^{-5}$
k (W/mk)	3.1	3.14
C_p (J/gK)	1.16	1.1721
T_m (°C)	1350	1450
L (km)	125	95

600 m above the predicted value) are eliminated. This mainly eliminates all the major seamounts and plateaus plus some hot-spot swells [13]. The ages are deduced from the map by Muller et al. [25]. The heat-flow values are those from the compilation by Stein and Abott [26].

In previous studies [4,5], the thermal parameters were adjusted to yield the best fit to the observed topography and heat-flow (Table 1). Here, the experimental data on the thermal parameters are taken into account. The computations were carried out using the fully temperature- and pressure-dependent coefficients given in Table 2 and discussed in Appendix C. This pressure and temperature dependence does much not affect the observables, as shown in Appendix C. On the other hand, the 'average value' of the coefficients (see definition in Appendix C) obviously matters. In inversions 1 and 2, α_m and $\bar{k}$ are allowed to vary around their experimentally found value: The parameters of Table 2 are multiplied by an arbitrary constant in order to yield the best fit to the observables, while the temperature- and pressure-dependent part is unchanged. The asymptotic plate thickness and the mantle temperature are left unconstrained. The mantle temperature is, however, expected to be around 1300°C from considerations on the fusion at the ridge [27].

Three inversions are performed and the three functions which are minimized are the following:

$$\sigma_t = \left(\alpha_e - \alpha_p \right)^2 / \sigma_\alpha^2 + \sigma_q + \sigma_d \quad \text{(inversion 1)}$$

$$\sigma_t = \left(k_e - k_p \right)^2 / \sigma_k^2 + \sigma_q + \sigma_d \quad \text{(inversion 2)}$$

$$\sigma_t = \sigma_q + \sigma_d \quad \text{(inversion 3)}$$

with:

$$\sigma_d = \sum_1^N \left(d_i - d_{ip} \right)^2 / \sigma_{d_i} \quad \text{and}$$

$$\sigma_q = \sum_1^M \left(q_i - q_{ip} \right)^2 / \sigma_{q_i}$$

In these expressions, the subscript p refers to 'predicted' values, that is, to the thermal coefficients or to the heat-flow or bathymetry predicted by the thermal lithospheric models (plate or CHABLIS); the subscript e refers to the experimentally obtained values for the thermal parameters; the subscript i refers to average of the observables for a 2 Ma interval, after 80 Ma, for the heat-flow and for a 1.7 Ma interval, between 0 and 180 Ma, for the topography. q_i and d_i are the average observed values for these time intervals. σ_{d_i} and σ_{q_i} are the dispersions around the average value, computed from the data for the topography or provided by Stein and Abott [27] for the heat-flow. σ_k is set equal to 0.7 W/mK and σ_α is set equal to 0.3 10^{-5} K^{-1}. In inversion 1, the average conductivity, $\bar{k}$, is fixed at 3.1 W/mK, in inversion 2, the 'average' thermal expansivity α_m is fixed at 3.85 10^{-5} K^{-1} and in inversion 3, $\bar{k}$ and α_m are fixed at 3.1 W/mK and 3.85 10^{-5} K^{-1}, respectively. The conductivity $k_1(T)$ is used for these inversions.

The results of the three inversions are given in Table 3. In case 1, the topography is slightly better

Table 2
Temperature- and pressure-dependent thermal parameters used in this study

$\alpha_m = 3.85 \ 10^{-5}$ K^{-1}	$\alpha(T,z) = \alpha_m(0.671 + 9.531 \cdot 10^{-4}T - 0.4844 \cdot 10^5 T^{-2}) \cdot (1 - 2.237 \cdot 10^{-4}z + 9.711 \cdot 10^{-8}z^2)^{5.6}$ (T in K, z in km)
$\bar{C}_p = 1.124$ J/gK	$C_p(T) = \bar{C}_p(-1.542 + 1.242 \cdot 10^{-5}T + 0.3322 \ln(T) + 0.3826 \cdot 10^3/T) - 1.217 \cdot 10^5/T^2 + 1.232 \cdot 10^7/T^3$ (T in K)
$\bar{k} = 3.1$ W/mK	$k_1(T) = \bar{k}(\dfrac{1}{0.518 + 7.89 \cdot 10^{-4}T} + 1.23 \cdot 10^{-10}T^3) \quad k_2(T) = \bar{k}(0.925 - 1.16510^{-4}T + 138.3/T)$

Table 3
Values of the best fitting coefficients found by inversion and associated variances in three cases

	Z_1 (km)	T_m(°C)	α_m (10^{-5} K^{-1})	$\bar{k}$ (W/mk)	σ_t	σ_d	σ_q
Case 1: α variable and $\bar{k}$ fixed							
Plate model	91	1430	3.34	fixed 3.1	3.9	2.4	2.5
CHABLIS model	105	1310	4.20	fixed 3.1	3.9	2.7	2.6
Case 2: α fixed and $\bar{k}$ variable							
Plate model	90	1280	fixed 3.85	3.3	4.2	2.8	2.9
CHABLIS model	117	1370	fixed 3.85	3.1	4.1	3.1	2.6
Case 3: α fixed and $\bar{k}$ fixed							
Plate model	82	1310	fixed 3.85	fixed 3.1	4.4	3.4	2.7
CHABLIS model	118	1350	fixed 3.85	fixed 3.1	4.1	3.1	2.6

Inversion 1: $\bar{k}$ fixed, α_m varied; inversion 2: α_m fixed, $\bar{k}$ varied; inversion 3: α_m and $\bar{k}$ fixed. σ_t, σ_q, and σ_d are defined in the text.
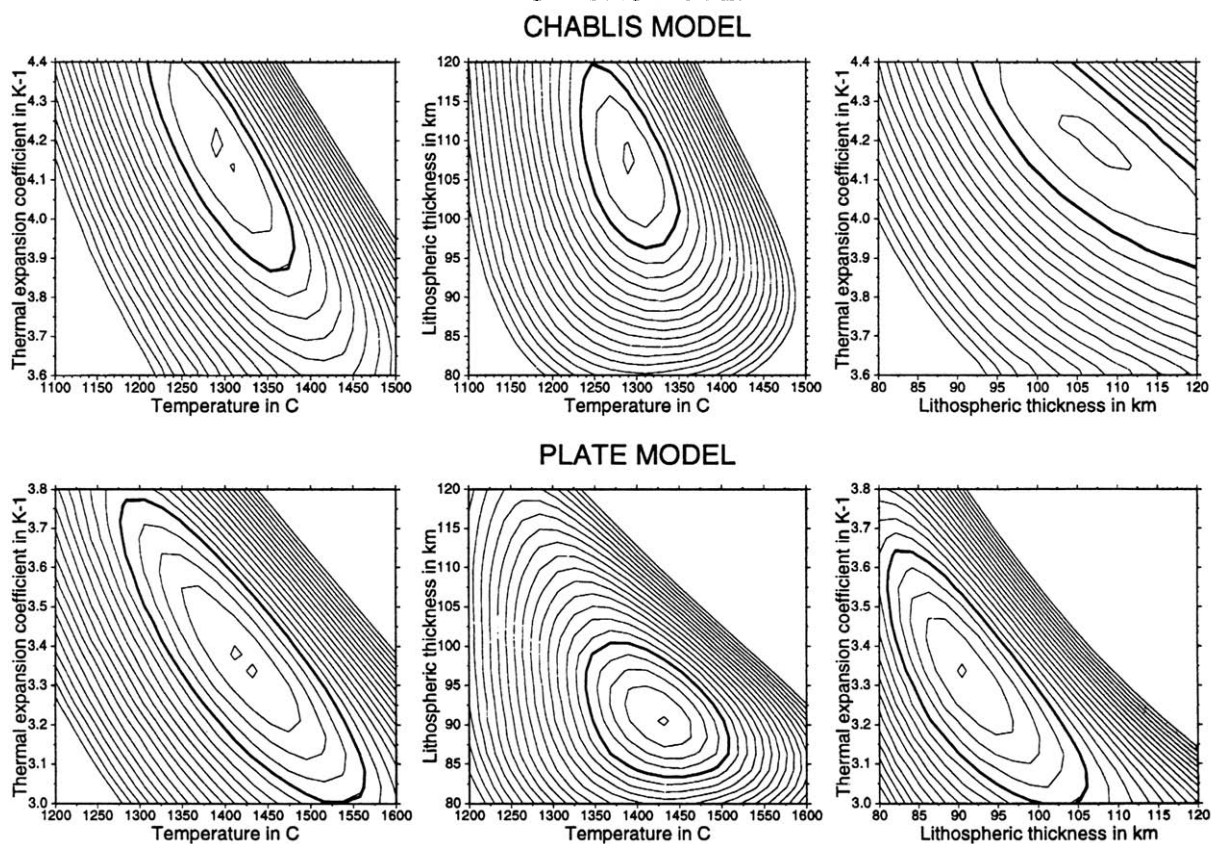
Fig. 2. Minimisation curves representing the function σ_t in planes passing through the minimum value. These curves correspond to inversion 1 of Table 3, both for the CHABLIS model (top) and the plate model (bottom). Fully temperature- and pressure-dependent parameters have been used in this inversion and the average thermal expansion coefficient is allowed to vary around the experimentally determined value. The average conductivity is fixed at 3.1 and the conductivity law $k_1(T)$ has been used. The spacing between isolines is 0.3. The thick line corresponds to the 1% confidence level for the parameters (F test).
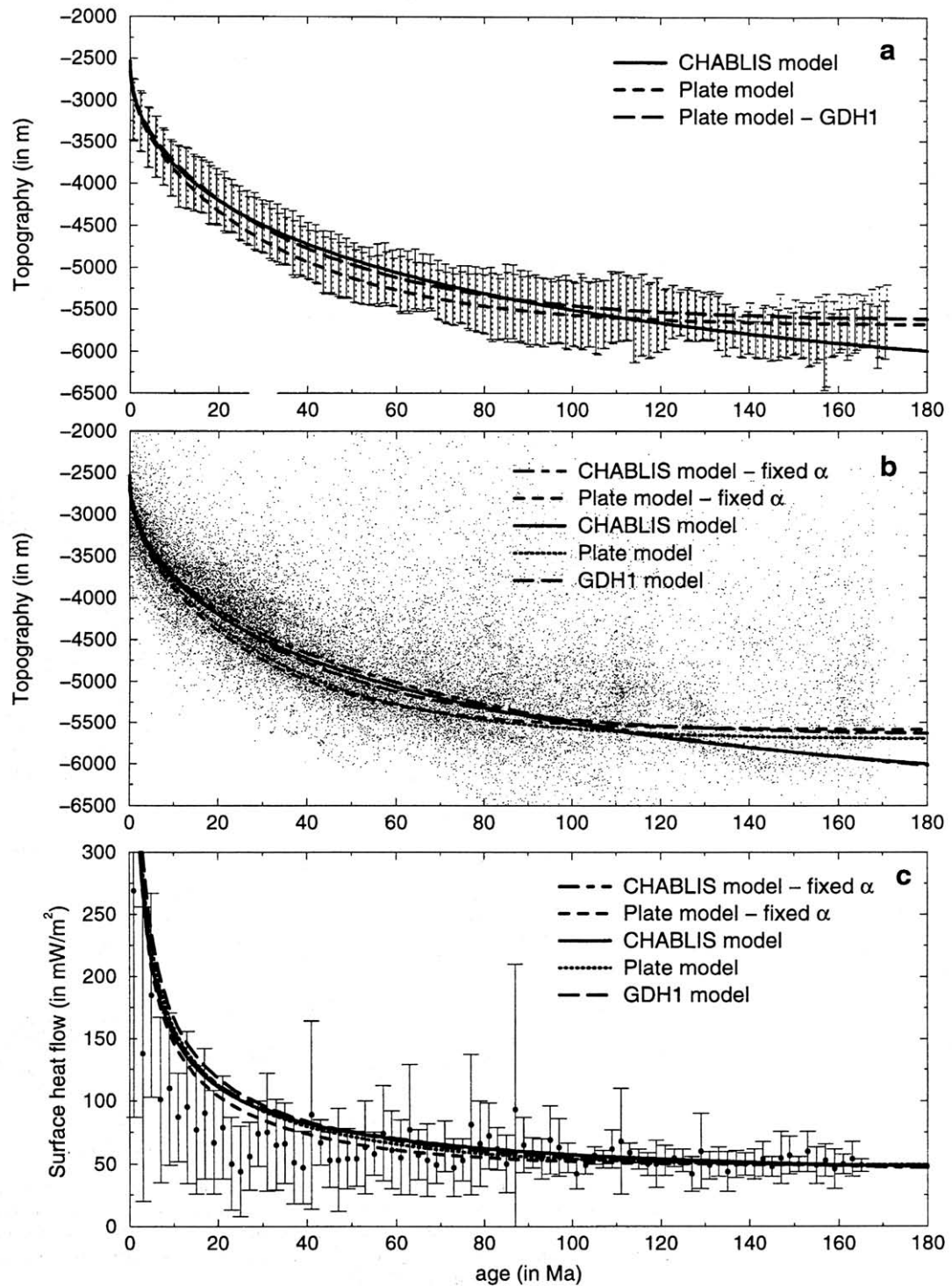
fitted by the plate model. The value of the predicted thermal expansion coefficient is, however, closer to the experimentally determined value for the CHABLIS model. Note that the plate model from inversion 1 is close to the GDH1 model. Its mantle temperature is large compared to that expected from considerations on fusion at the ridge. The global fit would be unfavourable to the plate model if a complementary term accounting for the deviation from expected mantle temperature was introduced in the inversion. In inversion 3, the bathymetry fits better with the CHABLIS model and the temperatures both for the plate and CHABLIS models are in the range of expected values. Letting the conductivity free to vary affects the results very little. The conductivity stays close to the experimentally determined value and the parameters from inversion 2 are almost similar to those obtained from inversion 3. Note that the best fitting value for the thermal expansion coefficient depends strongly upon the chosen model (plate or CHABLIS).

Fig. 2 shows σ_t 2-D cross-sections passing through the best fitting solution for inversion 1 both for the plate and the CHABLIS models, along with the 1% confidence level for the parameters. For a chosen model, a variation in the thermal expansion coefficient around the best-fit value, accompanied by variations in the opposite direction of the lithospheric thickness and mantle temperature, still yield acceptable solutions. Therefore, one cannot say that any of the parameters (lithospheric thickness, thermal expansion coefficient or mantle temperature) are constrained within better than 10% by the oceanic data.

3.2. Visual fit to the observables

The topography at young ages is often thought to follow very accurately a square root of age law. If this is so, then it is to be feared that the bathymetry
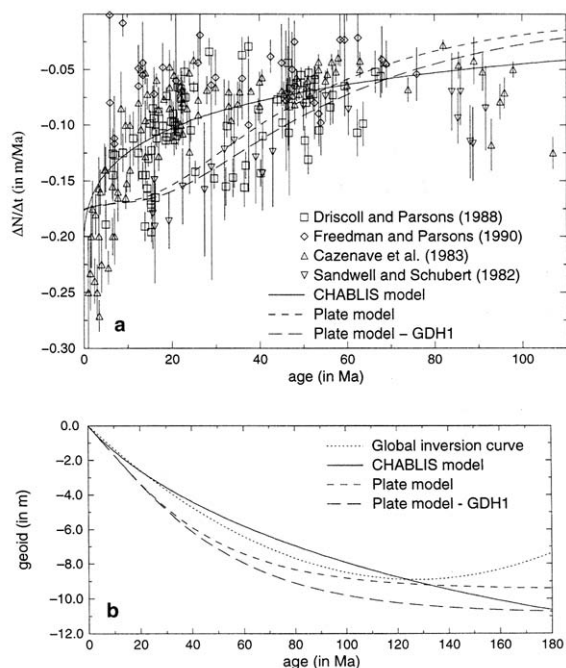

Fig. 4. Plate and CHABLIS models and fit to the geoid. (a) Geoid jump across transform faults divided by the age offset between the two sides of the fault [9,10,28,29] versus age, compared with the predictions of the GDH1 plate model and of the plate and CHABLIS models, with the parameters of inversion 1, Table 3. (b) Geoid function of age estimated from a global world inversion [11,12], compared with the predictions of the plate and CHABLIS models with the parameters of inversion 1, Table 3.

predicted by the CHABLIS model would not fit the data at young ages. Fig. 3a,b, as well as the dispersions reported in Table 3, show that this fear does not seem to be justified. The curves for the CHABLIS model and for the plate model always stay close to each other. Notice that the topography reaches its asymptotic value much earlier for the plate model than for the CHABLIS model (see Appendix C). Fig. 3c shows the heat-flow as function of age predicted by the plate and CHABLIS models. The heat-flow at

Fig. 3. Plate and CHABLIS models and fit to the observables. (a) Mean values and standard deviation in 1.7 Ma bins of the topographic data points used, compared with the topography predicted by the plate and CHABLIS models with the parameters of inversion 1 (see Table 3) and by the GDH1 plate model [5]. Observed world bathymetry (1° × 1°) (b) and heat-flow in 2 Ma bins (c) [27] compared with the topography and heat-flow predicted by the plate and CHABLIS models, with the parameters of inversion 1 and with the parameters of inversion 3 (see Table 3) and by the GDH1 plate model [5].

old ages is very well fitted by the two models. Only the heat-flow for ages larger than 80 Ma are introduced in the inversion because of the contamination of observations by water percolation problems at young ages.

Up to now, two determinations of geoid versus age have been given. The first one is based on the geoid jumps across transform faults [9,10,28,29]. Some of them are reported in Fig. 4a. They are compared with the geoid jumps predicted from the best fitting plate and CHABLIS models (case 1 of Table 3). As can be seen in Fig. 4a, there is a large dispersion of the data and both the CHABLIS and plate model seem to provide an acceptable fit, the CHABLIS model providing a slightly better fit at young ages. More recently [11,12], a global study of the geoid in the wavelength range corresponding to harmonics 4–10 has provided an estimate of the geoid function of age, parameterized by a function of shape $-a$age $+ b$age^2. The coefficients a and b were found to be equal to -0.14 m/Ma and $5.5 \cdot 10$ m^{-4}/Ma^2, respectively. In Fig. 4b, the CHABLIS model seems to yield a better fit to this geoid estimate. However, this better fit may come from the polynomial function chosen for the parameterization. We do not think that the geoid observations can be used to discriminate between the two models. They are simply compatible with both models.

3.3. The shape of the topography at young ages

The topography computed for the parameters of inversion 1 is well fitted by a curve $-431\sqrt{\text{age}} + 14 \cdot$ age. It does not follow a square root of age law, contrary to what is usually believed. In Fig. 5, the topography minus $14 \cdot$ age is plotted as function of the square root of age. It follows a linear trend. The young age shape of the oceanic topography appears to fit CHABLIS models well.

We also checked that the local topography taken along a flow line [30,31] could also be well fitted by the CHABLIS model. In spite of some obvious non-thermal effects, we found that the topography data along the various segments can be fitted well by a law $(a\sqrt{\text{age}} - b$age$)$, the coefficient a being kept equal to 431 and the coefficient b varying considerably from one area to the other. As mentioned in
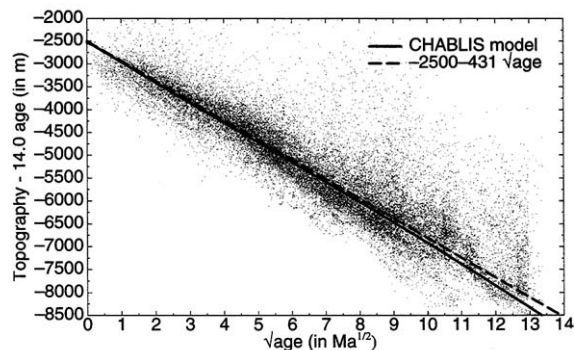

Fig. 5. Global topography minus 14·age. This figure illustrates the fact that the topography at young ages, usually thought to fit a linear trend as function of $\sqrt{\text{age}}$ also fits well a function of the type $a\sqrt{\text{age}} - b \cdot$age such as predicted by the CHABLIS model.

Appendix B, b is proportional to $\alpha_m q_b / (\rho_m - \rho_w) C_p$ where q_b represents the bottom heat-flow (Eq. (A1) in dimensional units). These variations in b can then be interpreted as variations of the bottom heat-flow. The difference of slopes is very difficult to explain in the framework of the plate model while the huge variations in heat-flow compatible with the CHABLIS model are likely to exist.

In summary, it has been shown in this section that the predictions from a CHABLIS model fit the observables at least as well as those from a plate model.

4. Discussion

4.1. The lithospheric thickness in the CHABLIS and plate model: intraplate volcanism and hot-spot swells

The asymptotic plate thicknesses are large for the CHABLIS model. However, at an age of 100 Ma, the plate and CHABLIS models are characterized by plates of similar thicknesses, of the order of 80 km, as shown in Fig. 6. This is very different from the lithospheric thicknesses of 100–120 km proposed in early models [4]. This reduced lithospheric thickness comes from the difference in the assumed thermal expansion coefficient and from the fact that the heat-flow in old oceanic basins is now estimated to be around 50 mW/m^2 [5]. The base of the lithosphere is now believed to be very close to the
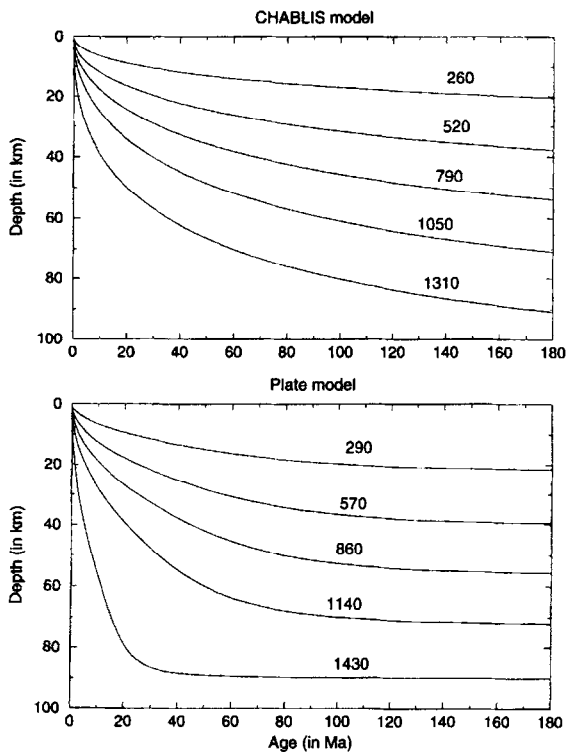
Fig. 6. Plate thickness and isotherms as function of age for the best-fit CHABLIS and plate models (inversion 1, Table 3).

spinel/garnet transition around which intraplate magmas are formed, as indicated by petrological and geochemical data [32]. On the other hand, the topographic swell around some hot-spots is very small, implying very little plate thinning. This was difficult to reconcile with previous large plate thicknesses but is perfectly consistent with the proposed thinner plates.

These depths, of the order of 70–80 km, also correspond to the depths where magma formation below the ridge begins. The material above that depth is then expected to be depleted and deprived of water. This could correspond to a zone of very high viscosity [33]. The convection would not penetrate the highly viscous and negatively buoyant matter, which is depleted. The depth of transition between depleted and non-depleted material would then be the 'base of the plate' and this depletion process provides some justifications for the plate model with a plate thickness around 80 km. The smaller slope of topography versus age when the ridge is shallower

(i.e., when the depleted layer is thicker) [30] may even find a justification in this context. This is, however, very speculative and, as discussed in the next section, poses problems for explaining the thermal subsidence of sedimentary basins after a stretching episode.

4.2. CHABLIS versus plate model: basin subsidence and seismic data

The main difference in behaviour between the plate and CHABLIS models comes from the subsidence at old ages (see Appendix B). For the plate model, the subsidence stops at about 80 Ma while, for the CHABLIS model, one fourth of the subsidence takes place after 80 Ma. Data on the sedimentary basins may yield constraints on the long term subsidence, provided that the same mechanism governs the asymptotic thickness of the lithosphere below continental and oceanic basins.

Up to now, the subsidence of most sedimentary basins has been analyzed using the plate model [34]. If what fixes the limit of the plate is the boundary between depleted and undepleted material, or any other petrological boundary, the adiabatically stretched lithosphere is in thermal equilibrium (except for a minor component linked to crustal radioactivity). Then no 'thermal subsidence' phase is expected, unless some volcanic activity has occurred and left some depleted material at the base of the lithosphere. The amount of subsidence would then depend upon the amount of melt produced but not upon the amount of stretching. If, on the other hand, the plate thickness is fixed by a convective process, such as cold blobs detaching from the more viscous lithosphere and sinking into the mantle, the appropriate boundary condition for modelling the long term evolution of the lithosphere might be a fixed heat-flux at the base of the plate (CHABLIS model) rather than a fixed temperature (plate model). In continents, because of the presence of a thick crust, the isotherms are shallower both because of the smaller crustal conductivity and because of the high radioactivity in the crust. For a similar heat-flow at the base of the plate the continents are expected to have an asymptotic plate thickness smaller than the oceans.

Basin subsidence can be affected by considerable

noise (such as: convective processes interacting with a heterogeneous lithosphere, non-local isostasy for the sedimentary load, temperature changes, etc.) and looking at the detailed data and history of each basin is beyond the scope of the present paper. Here, we simply discuss the tectonic subsidence of some basins older than 100 Ma. In the Paris basin [35], more than one third of the subsidence seems to have occurred during the past 120 Ma while extension stopped some 200 Ma ago. The latest stages of the evolution of the Paris basin are affected by perturbations in the near-by Massif Central area, so that it is difficult to derive more quantitative statements from this example. In Nova Scotia, the backstripped profiles [36], assuming no global sea level variations, indicate between 100 m and 400 m of subsidence during the last 100 Ma (i.e., 80 Ma after the stretching episode). Taking into account the sea level variations would somewhat increase the estimated tectonic subsidence. The back-stripped profiles for CoastB2 well, on the U.S. margin [37], also clearly show a long term subsidence. There, the stretching took place some 190 Ma ago. The total registered subsidence between 120 Ma and the present, amounting to more than 1000 m, is almost linear as function of time which, would be best compatible with a very long time constant. From these examples, it seems that there is a significant long term subsidence of the basins (i.e., subsidence continuing beyond 80 Ma after the stretching episode). In the framework of the plate model, this is not compatible with the thin plate thicknesses deduced from the old age heat-flow, the thermal expansivity and the topography as function of age in the oceans (GDH1 or Table 3 models). It is in better agreement with the predictions from the CHABLIS model, or from models with a continental plate much thicker than the oceanic one.

Recent seismic models of the upper mantle give constraints on the integral of the shallow temperature structure and detect a sizeable thickening of the oceanic lithosphere after 80 Ma [38,39]. This is compatible with the CHABLIS model but not with the plate model: according to the former model, the bathymetry, also proportional to the integral of the temperature anomaly, varies by about 900 m between 70 Ma and 180 Ma, as against 1700 m between 5 Ma and 70 Ma. In contrast, the deepening after 80 Ma is of 250 m or less for the plate model.

4.3. The CHABLIS model and the global heat budget of the mantle

The cooling of the mantle occurs partly through subduction (i.e., through the main convective system of plate tectonics), partly through small-scale convection. The relative importance of these two mechanisms for cooling the Earth is of interest for many general geodynamic problems, such as the thermal evolution of the Earth since the Archean [40] or the temperature structure in the present mantle, and can be computed easily. The heat budget through a lithospheric column is:

$$q_s = -\int_0^L \rho C_p \frac{\partial T}{\partial t} dz + q_b = q_c + q_b$$

where q_s represents the surface heat-flow and q_b the bottom heat-flow. At any given age, q_s can be decomposed into two parts: q_c is used to cool the plate and q_b corresponds to the heat exchanged by small-scale convection between the mantle and the plate. q_c will also ultimately be used to cool the mantle, but through the subduction process. Fig. 7 presents q_s and q_b for both the classical plate model and for the CHABLIS model. The difference between the two corresponds to q_c. Fig. 7a,b therefore gives for any lithospheric age a direct picture of the part of the surface heat-flow aimed at cooling the mantle through subduction (dark grey) and of the part of the heat-flow corresponding to cooling of the mantle through small-scale convection (light grey). By integrating these quantities over the Earth's surface; that is, by multiplying them by the oceanic area covered by lithosphere of a given age range (Fig. 7c), one obtains the relative importance of small-scale convection compared to plate-tectonic convection in the Earth's heat budget. If small-scale convection is effective below young oceans (CHABLIS model), it is a major agent in the cooling of the mantle, accounting for 40% of the heat transfer.

More data on the thermal expansivity as function of temperature would be necessary to assess definitely the validity of the CHABLIS model. However, it already appears to be a very reasonable alternative to the 'plate model'. Because it implies a different long-term subsidence and a much larger proportion of the cooling of the mantle by secondary convec-
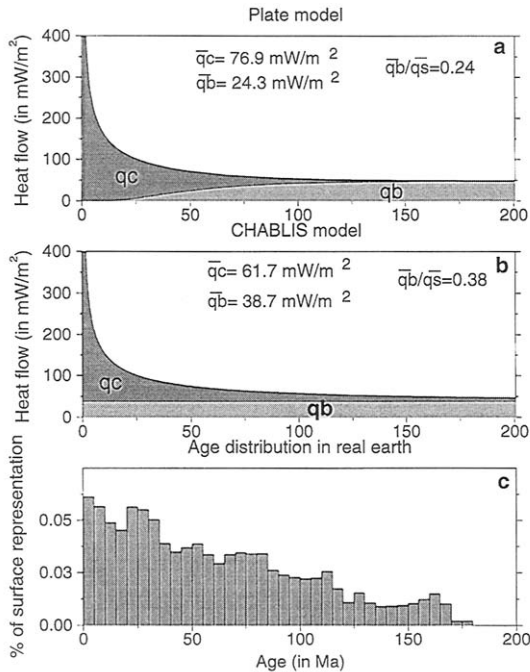
Fig. 7. Heat balance between primary and secondary convection. (a) The plate model. (b) The CHABLIS model. The upper curve (limit between dark grey and white) represents the surface heat-flow (q_s). The lower curve (limit between dark and light grey) represents the heat-flow at the base of the plate (q_b). The dark area represents the amount of coolness stored in the lithosphere per unit of time and area (q_c), while the light grey area represents the amount of coolness per unit of time and area transferred to the mantle by secondary convection (q_b). q_s represents the total amount of heat loss per unit of time and area. (c) The percent of the Earth's oceanic surface covered by plates of a given age range.

tion, this new type of model could affect current preconceptions about numerous mantle processes.

Acknowledgements

Appendix A. Oceanic topography and isostasy: a discussion

In this paper, the topography of the sea-floor is computed from the temperature in the lithosphere alone, assuming isostasy. In a number of previous studies [20,31,41,42], the topography due to cold blobs detached from the lithosphere is also taken into account. Does the material situated below the lithosphere induce sizable topography?

First, does secondary convection below the lithosphere really cool the mantle beneath it? In the framework of the CHABLIS model, the heat transfer, and hence the mantle temperature, must be independent of the age of the overlying lithosphere, as observed in convective models where a heat transfer from a hot lower boundary layer is introduced [18]. However, the plate model implies a heat transfer which depends on the age of the ocean. Many previous models took the very simplistic view that a blob always stays below the lithosphere it detaches from. A more realistic description would involve convective circulation in the mantle, with very large localized input of cold material near subduction zones, moderate widespread input of cold material under old oceans and no cold input below cratons and young oceans. In such a model, the mantle below old oceans might be statistically colder than below young oceans. The proximity of a subduction zone would, however, be the dominant factor.

Do deep density anomalies induce topography anomalies? The effect of secondary convection should be relatively small compared to the presence of added material in the neighbourhood of a subducting lithosphere. As subducting lithospheres do not seem to affect the oceanic topography [43], the same must be true for the cold blobs detached from the lithosphere. (It is, in fact, what is expected for two-layer or partially layered mantle convection).

Appendix B. Analytical considerations for the CHABLIS model

B.1. An approximate law for bathymetry versus age

One may wonder about the apparently very simple shape of the bathymetry versus age equation for the CHABLIS model:

$$\text{bathy} = a\sqrt{\text{age}} - b \cdot \text{age} \tag{A1}$$

The heat equation is:

$$\rho C_p \frac{\partial T}{\partial t} = k \frac{\partial^2 T}{\partial z^2} \qquad \text{(A2)}$$

where: ρ and C_p = the density and the calorific capacity; k = the conductivity; T = the temperature; and z = depth. For the CHABLIS model, this is solved with a temperature, T_0, fixed at the surface and with a flux, q_b, imposed on the bottom of the plate. If the temperature is made dimensionless by $(T_m - T_0)$ and the time by L^2/κ where $\kappa = k/\rho C_p$ and where L represents the final plate thickness, equal to $k(T_m - T_0)/q_b$, Eq. (A2) can be written as:

$$\frac{\partial T}{\partial t} = \frac{\partial^2 T}{\partial z^2} \qquad \text{(A3)}$$

with the boundary condition $(\partial T)/(\partial z) = 1$ on the plate bottom, where $T = 1$. There is a single solution to this equation, which is represented in Fig. 9. When non-dimensionalized by $(T_m - T_0) \, L\alpha \rho_m (\rho_m - \rho_w)$, the bathymetry can be written:

$$\text{bathy} = \int_0^1 (1 - T) \, dz \qquad \text{(A4)}$$

From Eq. (A3) and Eq. (A5), the increase in bathymetry during a lapse of time, dt, is found to be equal to the difference in surface minus bottom temperature gradient:

$$d(\text{bathy})/dt = (dT/dz)_{(z=0)} - 1 \qquad \text{(A5)}$$

The temperature field is the sum of two fields: one, T_1, corresponding to the cooling of an infinite half-space (the classical erf function), the second, T_2, corresponding to the effect of the heat-source, q_b, put at the bottom of the lithosphere. As a consequence, the surface heat flow corresponds to the heat-flow q_1 (equal to $1/\sqrt{\pi \text{age}}$) in non-dimensional units) plus a contribution, q_2, due the bottom heat source. If the bottom heat-flow was imposed at a depth proportional to the square root of age: $L = D\sqrt{\text{age}}$, then q_2 would be independent of age and
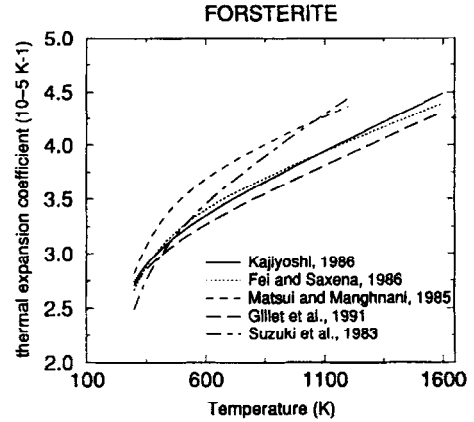
Fig. 8. Experimental data for the thermal expansivity of forsterite according to [44–48].

the total surface temperature gradient would be exactly:

$$\left(\frac{\partial T}{\partial z}\right)_{(z=0)} = 1/\sqrt{\pi \text{age}} + (1 - b) \qquad \text{(A6)}$$

where b depends on the coefficient D. After some algebra, b is found to be equal to:

$$b = \sqrt{\pi} \, (D/2) \exp(D^2/4) \text{erfc}(D/2)$$

Eq. (A6) and Eq. (A5) directly lead to Eq. (A1). In fact, the bottom of the lithosphere does not follow a square root of age law. This law is only approximate. However, as b varies only by some 10% in the range of the relevant values for D, the law (Eq. (A6)) for the surface temperature gradient function of age and, consequently, the law for the topography function of age are fairly well verified.

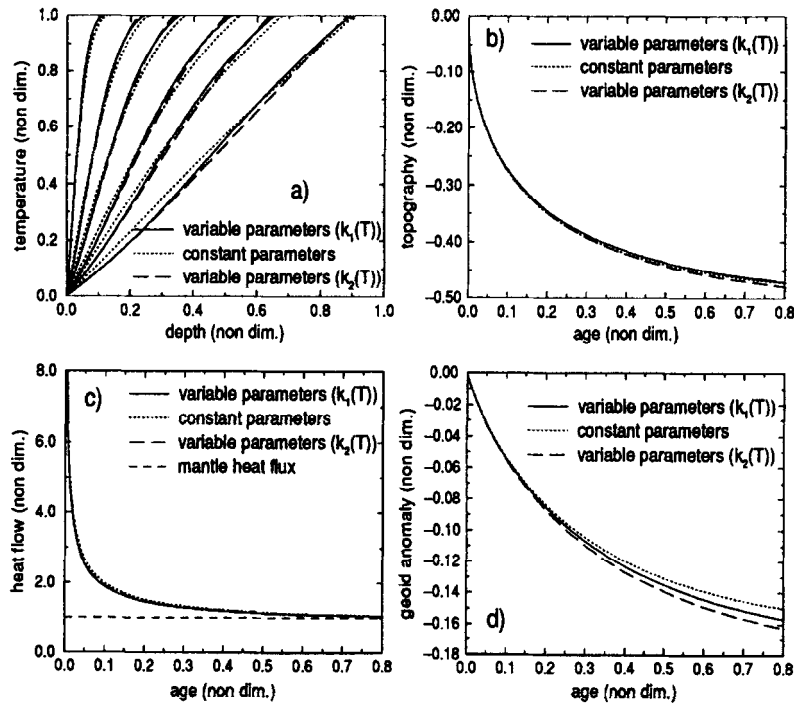### B.2. Long-term subsidence

For the plate model, the temperature is fixed between 0 and L. The difference between the asymptotic temperature and the temperature for a given age

---

Fig. 9. Influence of the thermal and pressure dependence of the thermal parameters (thermal conductivity, thermal expansion coefficient and heat capacity) on the evolution of the temperature profiles and on the observables (topography, heat-flow and geoid). The thermal parameters are given in Table 2. For the dotted curve, the fully temperature- and pressure-dependent values of Table 2, with the conductivities $k_1(T)$ or $k_2(T)$, have been replaced by their 'average' values noted in the left column of Table 2. The temperature profiles are presented for the non-dimensional times $t = 0.001$, 0.007, 0.02, 0.063, 0.132 and 0.51. Top = the plate model; bottom = the CHABLIS model.

PLATE MODEL
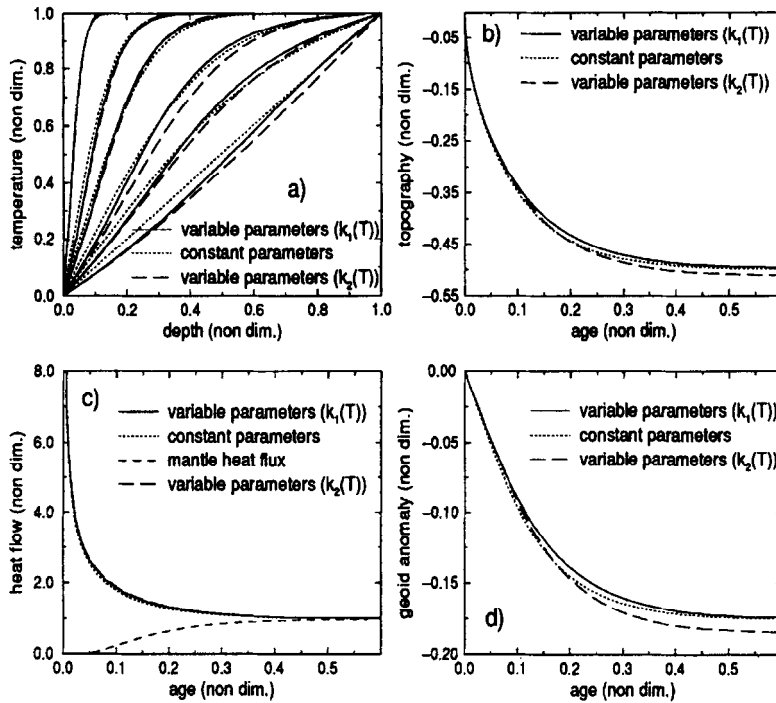
CHABLIS MODEL

can be approximated by a sinusoid with half period L [34]. The long-term subsidence then follows a law: $\exp(-\pi^2 t/L^2)$. For the CHABLIS model, the heat-flux is fixed at the base of the plate $z = L$ ($\partial T/\partial z = 1$ in non-dimensional units) and the temperature is fixed to unity in $z = 0$. According to the heat equation, $\partial T/\partial t = 0$ implies $\partial^2 T/\partial z^2 = 0$ in $z = 0$. Neglecting the higher-order harmonics, one may then write: $\partial T/\partial z = 1 + (\pi/2)(1/L - 1)\ \cos(\pi z/2L)$. The heat equation implies that, when L approaches 1, $(1/L - 1)$ varies as $a\ \exp(-\pi^2 t/4L^2)$. Neglecting the second-order terms in $\exp(-\pi^2 t/4L^2)$ and integrating twice, one obtains the topography:

$$\text{topo} = \frac{L^2}{2} - \frac{2a}{\pi} L^2 \exp\left(-\pi^2 t/4L^2\right)$$

$$= 0.5 - a(1 - 2/\pi)\exp\left(-\pi^2 t/4L^2\right)$$

This exponential dependence of the long-term subsidence is illustrated at the bottom of Fig. 1.

Appendix C. Temperature and pressure dependence of the material parameters

As shown in Fig. 8, a relatively large dispersion exists in the measurements of the thermal expansion coefficient of forsterite [44–48]. The data from Kajiyoshi [44] are used here. The thermal expansivity of other minerals are averaged in order to obtain a value characteristic of a rock with a mantle peridotite composition (see [12] for details). This temperature-dependent function is multiplied by a pressure-dependent term:

$$\alpha(p,T) = \beta(p)\gamma(T)$$

with $\beta(p) = (\rho/\rho_0)^\delta$. ρ_0 represents the density at zero pressure and ρ the density at the depth considered. δ is taken to be 5.6 [49]. The pressure variation is then modeled by the depth-dependent function:

$$\beta(p) = (1 - 2.237 \cdot 10^{-4} z + 9.711 \cdot 10^{-8} z^2)^\delta$$

where z is the depth in kilometres (see Table 2). This pressure dependence amounts only to a few percent for a 100 km thick lithosphere but affects the geoid anomaly. The experimentally determined thermal expansion coefficient appears to be larger than the values used in previous models. The calorific

capacities as a function of temperature measured for various minerals have also been averaged to yield the calorific capacity for a peridotitic composition (see [12] for details). The temperature dependence of this coefficient seems well constrained [50]. Two conductivity laws, $k_1(T)$ and $k_2(T)$, are tested here. The conductivity is the sum of lattice plus radiative conductivity. The lattice conductivity decreases with temperature and can be expressed as: $k_L = 1/(a + bT)$ while the radiative conductivity for a polycrystal follows the law $k_R = cT^3$. The coefficients a and b in the expression of k_L have been chosen in order to fit the data on measured thermal conductivity on peridotite (see [12] for details). The radiative conductivity has tentatively been set to $0.368 \cdot 10^{-9} T^3$ [12]. k_L plus k_R yield the conductivity law $k_1(T)$. As the estimate of the radiative conductivity is rather uncertain, we also performed models using the conductivity law $k_2(T)$ which decreases monotonously with temperature and gives a best fit through the experimentally measured values:

$$k_2(T) = 2.69 - 3.39 \cdot 10^{-4} T + 402.3/T$$

The pressure dependence of the conductivity and of the heat capacity are small and neglected in this paper.

The functions defining the various thermal coefficients can be written as the product of an 'average value' and a temperature-dependent part. The 'average' values are defined by:

$$\bar{k} = \frac{1}{(T_m - T_0)} \int_{T_0}^{T_m} k(T)\,dT$$

$$\bar{C_p} = \frac{1}{(T_m - T_0)} \int_{T_0}^{T_m} C_p(T)\,dT$$

$$\alpha_m = \frac{2}{(T_m - T_0)L} \int_0^L \int_{(T_m - T_0)z/L + T_0}^{T_m} \gamma(T)\,dT\,dz$$

The values for $\bar{k}$ and $\bar{C_p}$ indeed correspond to the average for a linear gradient. T_m has been chosen equal to 1330°C. α_m is such that it yields the same topography as a temperature-dependent parameter, if the temperature follows a linear gradient. The computations through the remainder of this paper are made using temperature- and pressure-dependent coefficients. However, we want to know if the possible

uncertainties on the temperature- and pressure-dependent part can considerably affect our conclusions. Fig. 9 presents predicted isotherms, topography, heat-flow and geoid as function of age. These quantities are plotted in non-dimensional units (see Appendix B). The geoid anomaly has been divided by $2 \pi \ GL^2 \ (T_m - T_0) \alpha_m \ \rho_m / g$. Note that the predicted values for the two main observables: topography versus age and heat-flow versus age, are almost not affected if one replaces the fully temperature- and pressure-dependent coefficients by their average values $\bar{k}$, $\bar{C}_p$ and α_m. The exact shape of the conductivity as a function of temperature affects the results relatively little. This is important because this shape is rather controversial.

References

[1] D.L. Turcotte and E.R. Oxburgh, Finite amplitude convective cells and continental drifts, J. Fluid Mech. 28, 29-42, 1967.

[2] D.P. McKenzie, Some remarks on heat flow and gravity anomalies, J. Geophys. Res. 72, 6261-6273, 1967.

[3] G. Schubert, C. Froidevaux and D.A. Yuen, Oceanic lithosphere and asthenosphere: Thermal and mechanical structure, J. Geophys. Res. 81, 3525-3540, 1976.

[4] B. Parsons and J.G. Sclater, An analysis of the variation of ocean floor bathymetry and heat flow with age, J. Geophys. Res. 82, 803-827, 1977.

[5] C.A. Stein and S. Stein, A model for the global variation in oceanic depth and heat flow lithospheric age, Nature 359, 123-129, 1992.

[6] G. Schubert and D.L. Turcotte, One dimensional model of shallow mantle convection, J. Geophys. Res. 77, 945-951, 1972.

[7] G. Schubert, D.A. Yuen, C. Froidevaux, L. Fleitout and M. Souriau, Mantle circulation with partial shallow return flow, J. Geophys. Res. 83, 745-758, 1978.

[8] B. Parsons and D. McKenzie, Mantle convection and the thermal structure of the plates, J. Geophys. Res. 83, 4485-4496, 1978.

[9] D.T. Sandwell and G. Schubert, Geoid height-age relation from SEASAT altimeter profiles across the Medocino fracture zone, J. Geophys. Res. 87, 3949-3958, 1982.

[10] A. Cazenave, B. Lago and K. Dominh, Thermal parameters of the oceanic lithosphere estimated from geoid height data, J. Geophys. Res. 88, 1105-1118, 1983.

[11] M.P. Doin, L. Feitout and D.P. Mckenzie, Geoid anomalies and the structure of continental and oceanic lithospheres, J. Geophys. Res., in press, 1996.

[12] M.P. Doin, Structure of the oceanic and continental lithosphere and gravity anomalies of the Earth. Ph.D. Thesis, Univ. Paris VI, 1995.

[13] P. Colin and L. Fleitout, Topography of the ocean floor:

Thermal evolution of the lithosphere and interaction of deep mantle heterogenities with the lithosphere, Geophys. Res. Lett. 17, 1961-1964, 1990.

[14] G.A. Houseman, D.P. McKenzie and P.H. Molnar, Convective instability of a thickened boundary layer and its relevance for the thermal evolution of continental convergent belts, J. Geophys. Res. 86, 6115-6132, 1981.

[15] D.A. Yuen and L. Fleitout, Stability of the oceanic lithosphere with variable viscosity: an initial-value approach, Phys. Earth Planet. Inter. 343, 173-185, 1984.

[16] A. Davaille and C. Jaupart, One set of thermal convection in fluids with temperature-dependant viscosity: Application to the oceanic mantle, J. Geophys. Res. 99, 19853-19866, 1994.

[17] W.R. Buck, When does small scale convection begin beneath oceanic lithosphere? Nature 313, 775-777, 1985.

[18] L. Fleitout and D. Yuen, Secondary convection and the growth of oceanic lithosphere, Phys. Earth Planet. Inter. 36, 181-212, 1984.

[19] W.F. Haxby and J.K. Weissel, Evidence for small scale convection from SEASAT altimeter data, J. Geophys. Res. 91, 3507-3520, 1986.

[20] W.R. Buck, Analysis of the cooling of a variable-viscosity fluid with applications to the Earth, Geophys. J.R. Astron. Soc. 89, 549-577, 1987.

[21] L. Fleitout and C. Moriceau, Short-wavelength geoid, bathymetry and convective pattern beneath the Pacific Ocean, Geophys. J. Int. 110, 6-28, 1992.

[22] S.T. Crough, Thermal model of oceanic lithosphere, Nature 256, 388-390, 1975.

[23] S.T. Crough, Approximate solutions for the formation of the lithosphere, Earth Planet. Sci. Lett. 14, 365-377, 1977.

[24] S.T. Crough and G.A. Thompson, Numerical and approximate solution for lithospheric thickening and thinning, Earth Planet. Sci. Lett. 31, 397-402, 1976.

[25] R.D. Muller, W.R. Roest, J.Y. Royer, L.M. Gahagan and J.G. Sclater, A digital age map of the ocean floor, SIO Ref. Ser. 93-30, 1993.

[26] C.A. Stein and D. Abbott, Heat flow constraints on the South Pacific superswell, J. Geophys. Res. 96, 16083-16100, 1991.

[27] D. McKenzie and M.J. Bickle, The volume and composition of melt generated by extension of the lithosphere, J. Petrol. 29, 625-679, 1988.

[28] M.L. Driscoll and B. Parsons, Cooling of the oceanic lithosphere — evidence from geoid anomalies across the Udintsev and Eltanin fracture zones, Earth Planet. Sci. Lett. 88, 289-307, 1988.

[29] A.P. Freedman and B. Parsons, Geoid anomalies over two South Atlantic fracture zones, Earth Planet. Sci. Lett. 100, 18-41, 1990.

[30] J.C. Marty and A. Cazenave, Regional variations in subsidence rate of oceanic plates: A global analysis, Earth Planet. Sci. Lett. 94, 301-315, 1989.

[31] M.A. Eberle and D.W. Forsyth, Regional viscosity variations, small-scale convection and the slope of the depth-age$^{1/2}$ curve, Geophys. Res. Lett. 22, 473-476, 1995.

[32] F. Albarcede, How deep do common basaltic magmas form and differentiate? J. Geophys. Res. 97, 10997-11009, 1992.

[33] G. Hirth and D.L. Kolsted, Are the oceanic lithosphere and asthenosphere separated by a compositional boundary, IUGG Abstracts B, 339, 1995.

[34] D.P. McKenzie, Some remarks on the development of sedimentary basins, Earth Planet. Sci. Lett. 40, 25–32, 1978.

[35] M.F. Brunet and X. Le Pichon, Subsidence of the Paris basin, J. Geophys. Res. 87, 8547–8560, 1982.

[36] L. Royden and C.E. Keen, Rifting process and thermal evolution of the continental margin of eastern Canada determined from subsidence curves, Earth Planet. Sci. Lett. 51, 343–361, 1980.

[37] M.S. Steckler and A.B. Watts, Subsidence of the Atlantic-type continental margin off New York, Earth Planet. Sci. Lett. 41, 1–13, 1978.

[38] H.C. Nataf and Y. Ricard, 3-SMAC: An a priori tomographic model of the upper mantle based on geophysical modelling, Phys. Earth Planet. Inter., in press, 1996.

[39] J.H. Woodhouse and J. Trmpert, Global crustal and mantle structure inferred from surface wave and other data, IUGG Abstracts B, 396, 1995.

[40] U.R. Christensen, Heat transport by variable viscosity convection and implications for the Earth's thermal evolution, Phys. Earth Planet. Inter. 35, 264–282, 1984.

[41] R.J. O'Connell and B.H. Hager, On the thermal state of the Earth, In: Physics of the Earth's Interior, A. Dziewonski and E. Boschi, eds., Proc. Enrico Fermi Int. Sch. Phys. 78, 270–317, 1980.

[42] G.F. Davies, Ocean bathymetry and mantle convection: 2 — Small-scale flow. J. Geophys. Res. 93, 10481–10488, 1988.

[43] P. Colin, Geoide global, topographie associeé et structure de la convection dans le manteau terrestre: modelisation et observations. Ph.D. Thesis, Univ. Paris 7, 1993.

[44] K. Kajiyoshi, High temperature equation of state for mantle minerals and their anharmonic properties, Ph.D. Thesis, Okayama Univ., 1986.

[45] I. Suzuki, O.L. Anderson and Y. Sumino, Elastic properties of a single crystal forsterite Mg_2SiO_4 up to 1200K, Phys. Chem. Miner. 10, 38–46, 1983.

[46] T. Matsui and M.H. Manghnani, Thermal expansion of a single crystal forsterite up to 1023K by Fizeau interferometry, Phys. Chem. Miner. 12, 201–210, 1985.

[47] P. Gillet, P. Richet, F. Guyot, and G. Fiquet, High temperature thermodynamic properties of forsterite, J Geophys. Res. 96, 11805–11816, 1991.

[48] Y. Fei and S.K. Saxena, A thermochemical data base for phase equilibria in the system Fe–Mg–Si–O at high pressure and temperature, Phys. Chem. Int. 13, 311–324, 1986.

[49] O.L. Anderson, D. Isaak and H. Oda, High-temperature elastic constant data on minerals relevant to geophysics, Rev. Geophys. 30, 57–90, 1992.

[50] P. Richet and G. Fiquet, High-temperature heat capacities and premelting of minerals in the system MgO–CaO–Al_2O_3–SiO_2, J. Geophys. Res. 96, 445–456, 1991.